Boletim da Sociedade Astronômica Brasileira, **32**, no. 1, 86-90

Identification of new quasars in the S-PLUS fields and determination of photo-zs using machine learning

L. M. I. Nakazono[1], C. Mendes de Oliveira[1], N. S. T. Hirata[2], S. Jeram[3], A. Gonzalez[3], S. Eikenberry[3], C. Queiroz[4], R. Abramo[4], & R. Overzier[5]

[1] Instituto de Astronomia, Geofísica e Ciências Atmosféricas da U. de São Paulo, Cidade Universitária, 05508-900, São Paulo, SP, Brazil. e-mail: lilianne.nakazono@usp.br
[2] Departamento de Ciência da Computação, Instituto de Matemática e Estatística da USP, Cidade Universitária, 05508-090, São Paulo, SP, Brazil
[3] Department of Astronomy, University of Florida, 211 Bryant Space Center, Gainesville, FL 32611, USA
[4] Departamento de Física Matemática, Instituto de Física, Universidade de São Paulo, SP, Rua do Matão 1371, São Paulo, Brazil
[5] Observatório Nacional / MCTIC, Rua General José Cristino 77, Rio de Janeiro, RJ, 20921-400, Brazil

Abstract. We present a methodology to identify stars, quasars and galaxies using data from the Southern Photometric Local Universe Survey (S-PLUS) in the Stripe-82 region. We compared the performance of two supervised learning algorithms: Support Vector Machine (SVM) and Random Forest (RF) in terms of precision, recall and F-measure. Tests were performed on a sample of 3 421 quasars, 13 228 stars and 21 181 galaxies, that were spectroscopically confirmed by SDSS. Statistical tests demonstrate that RF applied on 12 S-PLUS filters + 2 WISE bands (W1, W2) + Morphology parameters provided the best performance, due to inclusion of near-infrared information. We also consideredanything important to mention a second classifier trained only on 12 S-PLUS filters + Morphology parameters, as not all sources in the S-PLUS fields will have a WISE counterpart. In terms of quasar classification, we achieved 95.49% (92.83%) for precision and 95.26% (91.23%) for recall when considering a model with WISE (without WISE). For photometric redshift estimation, we obtained a precision of 6%, considering the feature space of 12 S-PLUS bands + 2 WISE bands in colors in a k-Nearest Neighbour algorithm. We conclude that the combination of S-PLUS and WISE filters is a powerful tool to search and determine photo-zs of new quasars.

Resumo. Neste trabalho apresentamos uma metodologia para identificar estrelas, quasares e galáxias usando dados do Southern Photometric Local Universe (S-PLUS) na região do Stripe-82. Comparamos a performance de dois algoritmos de classificação supervisionada: Support Vector Machine (SVM) e Random Forest (RF) em termos de precisão, *recall* e *F-measure*. Testes foram realizados em uma amostra de 3 421 quasares, 13 228 estrelas e 21 181 galáxias que foram confirmadas espectroscopicamente pelo SDSS. Testes estatísticos demonstraram que a melhor performance proveio do algoritmo RF aplicado no espaço de 12 filtros do S-PLUS + 2 bandas do WISE (W1, W2) + parâmetros morfológicos, dado a inclusão do infravermelho próximo. Também consideramos um segundo classificador treinado apenas no espaço de 12 filtros do S-PLUS + parâmetros morfológicos, devido à possibilidade de um objeto não ter sido observado pelo WISE. Em termos de classificação de quasares, obtivemos uma precisão de 95.49% (92.83%) e um *recall* de 95.26% (91.23%) quando considerado um modelo treinado com dados do WISE (sem WISE). Para o problema de regressão referente à estimação de *photo-zs*, a melhor precisão obtida foi de 6%, considerando as 12 bandas do S-PLUS e as 2 bandas do WISE em cores, utilizando k-Nearest Neighbours. Concluímos que a combinação de cores obtidas das bandas do S-PLUS e do WISE nos proporciona uma ferramenta poderosa para busca de quasares e determinação de seus *photo-zs*.

Keywords. quasars: general – Methods: statistical

1. Introduction

In this century, many telescopes have been or are being built to survey large areas on the sky, collecting data for an order of millions, and even billions of objects. For instance, GAIA DR2 (Gaia Collaboration et al., 2018) contains measurements of 1.7 billion sources; The Large Synoptic Survey Telescope (LSST; Ivezić et al., 2019) aims to provide 32 trillion observations of 40 billions objects. Object classification is a major issue for all these new surveys.

Generally, galaxies and stars can be easily separated due to their different morphologies (e.g. Moore et al., 2006, Pimbblet et al., 2001), while quasars can be confused with stars, given that both are unresolved sources. In the low signal-to-noise regime, however, galaxies and stars can also be difficult to separate. Object classification is best done when spectroscopy of the source is available, especially for emission-line galaxies, for which the classification is actually based on line widths (Baldwin et al., 1981,Lamareille, 2010, Kewley et al., 2006). However, spectroscopic surveys take so much longer for data collection than photometric surveys, many techniques have been developed to perform star/quasar separation on photometric surveys, such as: colour-colour cuts (e.g. Pâris et al., 2018, Schindler et al., 2017, Wu et al., 2012, Wu et al., 2010); proper motion criteria (e.g. Heintz et al., 2018, Guo et al., 2018); Bayesian Statistics (e.g. Yang et al., 2017, Peters et al., 2015, Kirkpatrick et al., 2011), and Machine Learning algorithms (e.g. Jin et al., 2019, Peng et al., 2012, Carrasco et al., 2015). Few works have tackled both problems at once in a 3-class (star/quasar/galaxy) separation (e.g. Kurcz et al., 2016, Yang et al., 2017, Clarke et al., 2019 – submitted). Brescia et al., 2015 have shown, using SDSS magnitudes, that a 3-class separation improved accuracy in comparison with a 2-step approach consisted of a galaxy/star and a star/qso classifications.

Object classification is highly facilitated if there are images available in a number of different filters, covering the whole spectral energy distribution, mimicking a low-resolution spectrum. In this sense, it is well known that combining optical

with infrared information (e.g. from WISE, Wright et al., 2010) greatly improves object classification (Wu et al., 2012, Schindler et al., 2017, Bovy et al., 2012). In addition, the narrow-bands surveys such as Javalambre-Physics of the Accelerated Universe Astrophysical Survey (J-PAS; Benitez et al., 2014), Javalambre Photometric Local Universe Survey (J-PLUS; Cenarro et al., 2019) and Southern Photometric Local Universe Survey (S-PLUS; Mendes de Oliveira et al., 2019) can be very useful to separate stars, quasars and galaxies, alone or combined with WISE data. In this work we use the data from S-PLUS, which covers 9300 deg^2 with the Javalambre optical filter system consisting of 7 narrow bands and 5 SDSS-like bands. We base our analysis on supervised learning algorithms to classify stars, quasars and galaxies in the S-PLUS fields of the first data release DR1, in the Stripe-82 area.

2. Database

2.1. Quasar selection

Among many wide-field spectroscopic surveys, the Sloan Digital Sky Survey (SDSS; York et al., 2000) has provided the largest amount of discovered quasars (hereafter QSOs). Recently, the quasar catalog from DR14 (DR14Q; Pâris et al., 2018) was released with 526 356 quasars over 9 376 deg^2. From the DR14, 16 261 quasars with $15 \leqslant r \leqslant 21$ fall over the Stripe-82 area. A cross-match between S-PLUS DR1 and DR14Q within 1 arcsec retrieves 14 054 (86.4% out of 16 261). If we restrict the sample only to the objects that have W1 and W2 valid data for magnitude, error and S/N, this number drops to 11 422 (70.2% out of 16 261) quasars (cross-matching was done using the AllWISE Source Catalogue within 2 arcsec). In this work we use a sample of quasars with no restriction in magnitudes, to enable assessment of the classification performance at the bright and faint end.

The final sample used had 13683 quasars with WISE counterpart and with any magnitude. The WISE magnitude information was taken directly from DR14Q and objects with null information on either magnitude, error or signal-to-noise, for the W1 and W2 bands, were excluded.

2.2. Star and galaxy selection

We selected all spectroscopically confirmed stars and galaxies down to a magnitude $r_{SDSS} = 22$ in Stripe-82 through a query in CasJobs[1], retrieving the spectroscopic and photometric information from the SDSS DR15. We cross-matched these catalogues of stars and galaxies with the AllWISE catalogue, within 2 arcsec, and then we cross-matched the resulting catalogue with the S-PLUS DR1, within 1 arcsec. Our final samples have 52 914 stars and 84 723 galaxies. Note that these only include objects that have WISE counterparts. If we only consider objects in the magnitude range $15 \leqslant r \leqslant 21$, they respectively represent 53.7% and 56% out of 96 894 stars and 147 289 galaxies from SDSS.

3. Methodology

3.1. Classification of stars, quasars and galaxies

We tested two different supervised learning algorithms for classification: Support Vector Machine (SVM) and Random Forest (RF). We implemented both algorithms from the `scikit-learn` (`sklearn`) library (Pedregosa et al., 2011) in Python.

[1] http://skyserver.sdss.org/CasJobs/

Several works have used the five SDSS broad-bands for either star/quasar or star/quasar/galaxy separation (e.g. Brescia et al., 2015, Peters et al., 2015). We want to evaluate the advantage of the 7 S-PLUS narrow-bands against using only the 5 broad-bands. Thus, we tested the following feature spaces:

(i) 12 S-PLUS bands
(ii) 12 S-PLUS bands + 2 WISE bands
(iii) 5 S-PLUS broad-bands
(iv) 5 S-PLUS broad-bands + 2 WISE bands

As we are considering fixed hyper-parameters for SVM and RF, we ended up with 8 unique experiments (4 feature spaces × 2 algorithms). For further references, we will call each experiment from its roman numeral (from the above list of feature spaces) followed by the letter *a*, for SVM, and *b*, for RF.

To evaluate the models, we consider metrics based on the confusion matrix. Considering $i, j \in \mathcal{Y}$, we can define precision (P) and recall (R) as follows:

$$P_i = \frac{(TP)_i}{(TP)_i + \sum_{j \neq i} (FP)_{i,j}} \tag{1}$$

$$R_i = \frac{(TP)_i}{(TP)_i + \sum_{j \neq i} (FN)_{i,j}} \tag{2}$$

In Astronomy, precision is also known as purity and recall is also known as completeness or efficiency. We can also define another metric that evaluates R and P in a single value, which is the harmonic mean of P_i and R_i called as F-measure (F_i):

$$F_i = 2\left(P_i^{-1} + R_i^{-1}\right)^{-1} = 2 \times \frac{P_i R_i}{P_i + R_i}. \tag{3}$$

Note that P_i, R_i and $F_i \in [0,1]$. For the goal of this project, we expect P_i, R_i and, consequently, F_i to be ≈ 1. For an overall evaluation of the model's performance (i.e. considering the classification of quasars, stars and galaxies altogether), we use the macro-averaged F-measure ($\bar{F}$), defined as the mean of the F-measure values.

3.2. Photo-z determination for quasars candidates

We estimate one photo-z by measuring the median of the spectroscopic redshifts of the n-th closest spectroscopically confirmed quasars from the corresponding quasar candidate. This method is also called as k-Nearest Neighbours (kNN). We use the implementation from `sklearn.neighbors.NearestNeighbors` with all parameters set as default.

We divided our quasar sample into 70% as training set and 30% as testing set, using `sklearn.train_test_split` with `random_state = 42`. We end up with 9 639 quasars in training set and 4 132 quasars in testing set.

We compare the performance of kNn on the same features spaces (i) to (iv) described in §3.1 along with 4 more feature spaces:

(v) 12 S-PLUS bands in colors: uJAVA − g, J0378 − g, J0395 − g, J0410 − g, J0430 − g, g magnitude , g − J0515, g − r, g − J0660 , g − i, j − J0861, g
(vi) 12 S-PLUS bands + 2 WISE bands in colors: as (vi) with additional g − W1 and g − W2
(vii) 5 S-PLUS broad-bands in colors: u − g, g − r, r − i, i − z

Table 1. Classification results using SVM and RF without restrictions (e.g. signal-to-noise, missing values, limiting magnitudes, etc.). The letters Q, S and G stand for quasar, star and galaxy, respectively.

Features	Algorithm and Training time (s)	Class	Precision	Recall	F-measure
(i) 12 S-PLUS bands: uJAVA, J0378, J0395, J0410, J0430, J0515, J0660, J0861, g, r, i and z	(b) SVM 263.6193 ± 17.1576	Q	0.7847 ± 0.0054	0.927 ± 0.0023	0.85 ± 0.0031
		S	0.9119 ± 0.0041	0.8952 ± 0.0043	0.9034 ± 0.0015
		G	0.9275 ± 0.0021	0.9109 ± 0.0029	0.9191 ± 0.0007
		Macro-averaged F-measure: 0.8908 ± 0.0013			
	(b) RF 19.5892 ± 1.3423	Q	0.909 ± 0.0057	0.8749 ± 0.0037	0.8916 ± 0.0034
		S	0.9587 ± 0.0022	0.9005 ± 0.0052	0.9287 ± 0.002
		G	0.9243 ± 0.0027	0.9649 ± 0.0014	0.9441 ± 0.0009
		Macro-averaged F-measure: 0.9215 ± 0.0014			
(ii) 12 S-PLUS bands + 2 WISE bands: uJAVA, J0378, J0395, J0410, J0430, J0515, J0660, J0861, g, r, i, z, W1 and W2	(b) SVM 199.7843 ± 18.3514	Q	0.9052 ± 0.0019	0.955 ± 0.0028	0.9294 ± 0.0022
		S	0.9588 ± 0.0017	0.9525 ± 0.0032	0.9556 ± 0.0017
		G	0.965 ± 0.0019	0.9603 ± 0.0011	0.9626 ± 0.001
		Macro-averaged F-measure: 0.9492 ± 0.0011			
	(b) RF 19.3189 ± 0.0919	Q	0.951 ± 0.004	0.9367 ± 0.0046	0.9438 ± 0.0026
		S	0.9698 ± 0.0013	0.9659 ± 0.002	0.9678 ± 0.0011
		G	0.9701 ± 0.0013	0.9749 ± 0.001	0.9725 ± 0.0007
		Macro-averaged F-measure: 0.9614 ± 0.0011			
(iii) 5 S-PLUS broad-bands: uJAVA, g, r, i, z	(b) SVM 136.9018 ± 13.5146	Q	0.753 ± 0.008	0.9378 ± 0.0023	0.8353 ± 0.0051
		S	0.8985 ± 0.0031	0.8927 ± 0.003	0.8956 ± 0.0019
		G	0.9259 ± 0.0017	0.8928 ± 0.0027	0.9091 ± 0.0015
		Macro-averaged F-measure: 0.88 ± 0.0024			
	(b) RF 11.7195 ± 0.1905	Q	0.8936 ± 0.0052	0.8578 ± 0.0054	0.8753 ± 0.0039
		S	0.9256 ± 0.0024	0.8836 ± 0.0046	0.9041 ± 0.0022
		G	0.9111 ± 0.0026	0.9428 ± 0.0015	0.9267 ± 0.0009
		Macro-averaged F-measure: 0.902 ± 0.0013			
(iv) 5 S-PLUS broad-bands + 2 WISE bands: uJAVA, g, r, i, z, W1 and W2	(b) SVM 55.9284 ± 5.2862	Q	0.8987 ± 0.0064	0.9773 ± 0.0034	0.9363 ± 0.0045
		S	0.9616 ± 0.0015	0.9694 ± 0.0022	0.9655 ± 0.0013
		G	0.979 ± 0.0015	0.9601 ± 0.001	0.9695 ± 0.0011
		Macro-averaged F-measure: 0.9571 ± 0.0021			
	(b) RF 14.2676 ± 1.0016	Q	0.9488 ± 0.0038	0.9411 ± 0.0029	0.945 ± 0.0014
		S	0.9641 ± 0.0015	0.9641 ± 0.0022	0.9641 ± 0.0012
		G	0.9695 ± 0.0015	0.9708 ± 0.0008	0.9702 ± 0.0007
		Macro-averaged F-measure: 0.9597 ± 0.001			

(viii) 5 S-PLUS broad-brands + 2 WISE bands in colors: as (v) with additional g − W1 and g − W2

In order to assess the performance of this method, we calculate the NMAD defined in Equation 4:

$$\sigma_z = 1.48 \times \text{median}\left(\frac{|\delta z - \text{median}(\delta z)|}{1 + z_s}\right), \quad (4)$$

with $\delta z = \tilde{z} - z_s$, where z_s denotes the spectroscopic redshift, and $\tilde{z}$ is the photometric redshift.

4. Results

4.1. Classification of stars, quasars and galaxies

Results for each model experiment are shown in Tab. 1. We compared their performances through unpaired two-sample t-tests, which are not shown in this proceeding. Firstly, we evaluated that the RF significantly improves the classification, compared to SVM. We can see that, generally, RF requires less than 10% of the SVM's computational time. Thus, we will only consider results from RF for the further tests.

One aim of this work is to assess if the narrow-bands improve the classification. Then we compared i-b with iii-b, i.e. when WISE magnitudes are not being considered, and ii-b with iv-b, when considering WISE magnitudes. With addition of WISE, the narrow-bands do not significantly increase (or decrease) the performance of quasar classification. This is possibly due to the fact that WISE plays a more important role on distinguishing objects. However, star precision and galaxy recall have been significantly improved. On the other hand, the S-PLUS narrow-bands significantly increase the precision and recall of all classes when training RF without WISE magnitudes, showing that a good star/quasar/galaxy classification is achieved also with the 12 bands only. This is important to note, given that we do not have WISE detection for all sources. Nevertheless, we evaluated the inclusion of W1 and W2 by comparing i-b with ii-b and iii-b with iv-b, confirming the importance of WISE magnitudes for the classification. The best feature spaces with and without WISE in a RF algorithm are 12 S-PLUS bands (i) and 12 S-PLUS bands + 2 WISE bands (ii), respectively.

Costa-Duarte et al., 2019 (submitted) concluded that using a RF algorithm with a combination of the 12 S-PLUS filters plus information on object morphology increases the accuracy of the star/galaxy classification. Thus, we also included morphology information in our training in an attempt to improve the performances. The parameters `FWHM`, `A`, `B` and `KrRadDet` were included within the experiment i-b and ii-b and we will further refer to them as i-b* and ii-b*. The results including morphology statistically improved the star/galaxy classification for both experiments, as already expected (Tables 3 and 2). Moreover, the precision and recall for all classes significantly increased, for the case when WISE information is used, as compared to no WISE

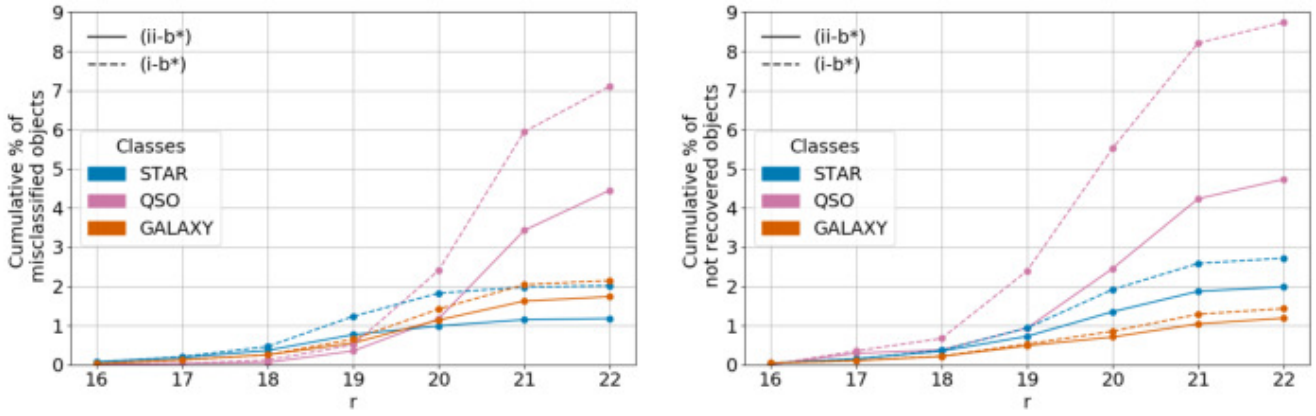

Figure 1. Cumulative percentages of misclassified and not recovered stars (blue), quasars (pink) and galaxies (orange). The models referring to 12 S-PLUS bands + 2 WISE bands + Morphology features (ii-b*) and 12 S-PLUS bands + Morphology (i-b*) features in a Random Forest algorithm are represented by a solid and dashed curves, respectively. (a) Cumulative percentage of misclassified objects per magnitude. The fraction's denominators are the total of predictions in each class, therefore it may vary from classifier to classifier. For ii-b* (i-b*), we are calculating the fractions from a total of 13 111 (13 121) star, 3 406 (3 353) quasar and 21 313 (21 356) galaxy classifications. (b) Cumulative percentage of not recovered objects per magnitude from a total of 13 228 known stars, 3 421 known quasars and 21 181 known galaxies.

Table 2. Cross-validation results for the experiment i-b* with morphology inclusion, i.e. considering the feature space consisted of 12 S-PLUS bands + Morphology within a Random Forest algorithm with 100 estimators and bootstrap.

Class	Precision (P)	Recall (R)	F-measure (F)
QSO	0.9286 ± 0.0044	0.9135 ± 0.0051	0.9210 ± 0.0038
STAR	0.9803 ± 0.0016	0.9716 ± 0.0022	0.9759 ± 0.001
GALAXY	0.9773 ± 0.0007	0.9853 ± 0.0008	0.9813 ± 0.0003
Macro-averaged F-measure ($\bar{F}$): 0.9594 ± 0.0011			
Fit time: 23.8817 ± 0.4656s			

Table 3. Cross-validation results for the experiment ii-b* with morphology inclusion, i.e. considering the feature space consisted of 12 S-PLUS bands + 2 WISE bands + Morphology within a Random Forest algorithm with 100 estimators and bootstrap.

Class	Precision (P)	Recall (R)	F-measure (F)
QSO	0.9522 ± 0.0058	0.9516 ± 0.0024	0.9519 ± 0.0024
STAR	0.9886 ± 0.0016	0.9789 ± 0.0023	0.9837 ± 0.0008
GALAXY	0.9820 ± 0.0013	0.9881 ± 0.0007	0.9850 ± 0.0006
Macro-averaged F-measure ($\bar{F}$): 0.9735 ± 0.0011			
Fit time: 26.614 ± 1.1522s			

information, except for the QSO precision (the latter case does not show a significant statistical difference).

After this step of model validation, we calculated the expected precision and recall for the two different classifiers using the testing set. The final model performances can be checked in Fig.1. Fig. 1(a) shows the cumulative percentage of mistakes (i.e. $1 - P_i$) in the classification per model, per class and per magnitude in r. The cumulative misclassification rates of quasars, stars and galaxies ares 0.35% (0.50%), 0.77% (1.23%) and 0.55% (0.65%) for ii-b* (i-b*) at magnitude r = 19, respectively. Furthermore, the star/QSO/galaxy separation is still reasonable good up to magnitude r = 22, specially for galaxies and stars, for which misclassification rates remain slightly constant. On other hand, a steep increase in our quasar classification errors can be seen for both models, but specially for model i-b*. In Fig 1(b) we show the cumulative percentage of not recovered objects (i.e. $1 - R_i$) per model, per class and per magnitude in r. We can see that a lot more quasars are not being recovered with model i-b* in comparison to model ii-b* even at lower magnitudes. Up to magnitude r = 19, the rates are 0.93% (2.40%), 0.72% (0.94%) and 0.49% (0.53%) for quasars, stars and galaxies, respectively. At fainter magnitudes the rates of not recovered stars and galaxies remain fairly good.

4.2. Photo-z determination for quasars candidates

The best precision achieved is $\sigma_z = 6.56\%$ considering $k = 5$ when training k-NN within the feature space 12 S-PLUS bands + 2 WISE bands in colors. In overall, this feature space provided a better performance in comparison with others (Fig. 2). The exception occurs in the bright and faint end of magnitude, which is mainly due to a lack of observed quasars at r < 17 and r > 21. Thus, this precision can only be improved if we can increase the number of observed data at these ranges of magnitude. We reach a precision of 6.33% when only considering objects in the range $17 \leq r < 18$, 3.54% for $18 \leq r < 19$ and 3.66% for $19 \leq r < 20$. In terms of spectroscopic redshift, we achieved the lowest σ_z of 2.44% for objects within $2 \leq z < 3$. For objects within $0 \leq z < 1$, $1 \leq z < 2$ and $z \geq 3$ we achieved, respectively: 7.26%, 8.51% and 5.22%.

5. Conclusions

After several tests, we selected two models for classifying stars, quasars and galaxies in the S-PLUS fields:

- Classifier i-b*: 12 S-PLUS bands + Morphology parameters within a Random Forest algorithm with 100 estimators and bootstrap
- Classifier ii-b*: 12 S-PLUS bands + 2 WISE bands + Morphology parameters within a Random Forest algorithm with 100 estimators and bootstrap

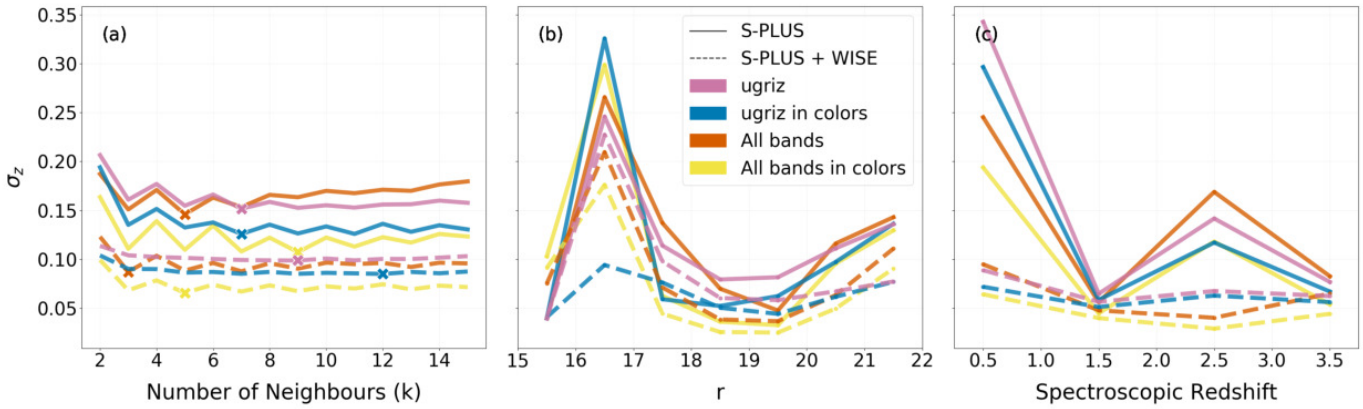

Figure 2. Relation between σ_z and: (a) number of neighbours, where the markers represent the best precision found, (b) magnitude in r and (c) spectroscopic redshift. Each color correspond to a different feature space: 12 S-PLUS bands (red), 12 S-PLUS bands in colors (yellow), 5 S-PLUS broad-bands (pink) and 5 S-PLUS broad-bands in colors (blue). The dashed lines represent the feature spaces that includes W1 and W2 from WISE.

Considering ii-b* (i-b*), we achieved a macro-averaged F-measure of 97.44% (95.95%). In terms of quasar classification, we achieved 95.49% (92.83%) for precision, i.e., 121 (149) galaxies and 34 (93) stars were wrongly classified as quasars. Meanwhile, we achieved 95.26% (91.23%) for recall, i.e., 142 (194) quasars were classified as galaxies and 21 (107) quasars was classified as star. In terms of star classification, we got a precision of 98.82% (97.98%) and recall of 98% (97.26%). Finally for galaxies, a precision of 98.26% (97.83%) and a recall of 98.8% (98.56%) were obtained. Specifically, 230 (269) stars were classified as galaxies and 134 (158) galaxies were classified as stars. We concluded that the narrow-bands improve the star/quasar/galaxy classification, especially when no WISE information is available. In terms of estimating photometric redshifts of our quasars candidates, we achieved the best performance (σ_z = 6.56%) for kNN when considering the 12 S-PLUS bands + 2 WISE bands in colors.

References

Baldwin, J. A. et al. (1981). *PASP* 93, pp. 5–19.
Benitez, N. et al. (2014). *arXiv e-prints*, arXiv:1403.5237, arXiv:1403.5237.
Bovy, Jo et al. (2012). *The Astrophysical Journal* 749.1, p. 41.
Brescia, M. et al. (2015). *Monthly Notices of the Royal Astronomical Society* 450.4, pp. 3893–3903.
Carrasco, D. et al. (2015). *Astronomy Astrophysics* 584, A44.
Cenarro, A. J. et al. (2019). *A&A* 622, A176, A176.
Clarke, A. O. et al. (2019).
Costa-Duarte, M. V. et al. (2019).
Gaia Collaboration et al. (2018). *A&A* 616, A1, A1.
Guo, Sufen et al. (2018). *Astronomy Astrophysics* 618, A144.
Heintz, K. E. et al. (2018). *A&A* 615, L8, p. L8.
Ivezić, Željko et al. (2019). *The Astrophysical Journal* 873.2, p. 111.
Jin, Xin et al. (2019). *MNRAS* 485.4, pp. 4539–4549.
Kewley, L. J. et al. (2006). *MNRAS* 372, pp. 961–976.
Kirkpatrick, Jessica A. et al. (2011). *The Astrophysical Journal* 743.2, p. 125.
Kurcz, A. et al. (2016). *Astronomy Astrophysics* 592, A25.
Lamareille, F. (2010). *A&A* 509, A53, A53.
Mendes de Oliveira, C. et al. (2019). *MNRAS* 489.1, pp. 241–267.
Moore, Jason A. et al. (2006). *Publications of the Astronomical Society of Australia* 23.04, pp. 135–146.
Pâris, I. et al. (2018). *A&A* 613.A51.
Pedregosa, F. et al. (2011). *Journal of Machine Learning Research* 12, pp. 2825–2830.
Peng, Nanbo et al. (2012). *MNRAS* 425.4, pp. 2599–2609.
Peters, C. M. et al. (2015). *ApJ* 811, 95, p. 95.
Pimbblet, K. A. et al. (2001). *Monthly Notices of the Royal Astronomical Society* 327.2, 588–600.
Schindler, Jan-Torge et al. (2017). *ApJ* 851, 13, p. 13.
Wright, Edward L. et al. (2010). *AJ* 140.6, pp. 1868–1881.
Wu, Xue-Bing et al. (2010). *Monthly Notices of the Royal Astronomical Society*, no–no.
Wu, Xue-Bing et al. (2012). *AJ* 144, 49, p. 49.
Yang, Qian et al. (2017). *AJ* 154, 269, p. 269.
Yang, Qian et al. (2017). *The Astronomical Journal* 154.6, p. 269.
York, D. G. et al. (2000). *AJ* 120, pp. 1579–1587.